JOURNAL OF GEOPHYSICAL RESEARCH, VOL. 100, NO. A11, PAGES 21,385–21,396, NOVEMBER 1, 1995

Imaging of artificial aurora in the upper atmosphere

S. B. Mende, S. A. Fuselier, S. P. Geller, and G. R. Swenson
Lockheed Palo Alto Research Laboratory, Palo Alto, California

J. A. Marshall
Department of Physics, Utah State University, Logan

Abstract. We use continuum (white light) and filtered (427.8 nm) images from the Atmospheric Emissions Photometric Imaging (AEPI) experiment on the Atmospheric Laboratory for Applications and Science (ATLAS) 1 shuttle mission to investigate the shape and evolution of artificial auroral patches generated by the Space Experiments with Particle Accelerators (SEPAC) electron beam experiment. Auroral patches generated by this beam experiment are complex and differ in the white light and filtered images. In the white light images, the auroral patch consists of a relatively large, diffuse, and somewhat symmetric head and a tail that is directed approximately opposite the spacecraft velocity vector. From the growth of the tail during a beam pulse, the distance from the imager to the emissions is estimated to be about 200 km, consistent with expectations from a simple model of auroral emissions in the atmosphere. In addition to the auroral patch, an intense, diffuse, and variable background glow filling essentially the entire field of view of the white light imager is seen during the beam pulses. This background glow may be caused by low-energy electrons very near the shuttle. This glow is absent in the filtered images, in which the shape of the auroral patch differed, consisting of a relatively large, diffuse, but more asymmetric head, a tail, and a smaller and less intense spot below the head. Curvature of the magnetic field and spacecraft motion during the 1-s filtered images allows an estimate of the relative distance from the shuttle to the head, tail, and small spot. This shape is consistent with head emissions generated relatively near the spacecraft (nearest few kilometers), tail emissions somewhat farther away, and finally the small spot emissions generated the farthest away in the lower atmosphere where the natural auroras would be created. In addition, the shape of these patches in the filtered images suggests that the risetime for the head and tail emissions in the filtered images appears to be longer than that for the small spot emission. The differences between the white light images and the filtered images are consistent with the difference between the emission parent state lifetimes and the energy requirement for the emission production. The white light images contain emissions with long lifetimes, and these emissions which are produced near the observer are swept out of the field of view because they are left behind by the shuttle. This gives a bias toward emissions generated farther from the orbiter. The filtered images contain only the very fast produced N_2^+ emission with a substantial component generated near the orbiter and with an inverse square law attenuated auroral spot in the lower atmosphere. The presence of the tail and the apparent risetime in the near-field emission suggest that there is a buildup and decay time associated with the hot plasma created by the electron beam.

Introduction

The Earth's aurora are created by the precipitation of energetic (several keV) electrons and ions into the upper atmosphere. Understanding the generation of these emissions in the upper atmosphere requires determination of the precipitating charged particles as well as an understanding of the interactions between these particles and the ions and neutrals in the upper atmosphere.

One way to reduce the unknown quantities of this complex interaction is to perform controlled experiments where electron beams of known energy and flux are injected into the upper atmosphere. Several rocket experiments carrying electron accelerators have successfully generated artificial aurora in this manner [e.g., *Hess et al.*, 1971; *Davis et al.*, 1971; *Hallinan et al.*, 1978, 1990; *O'Neil et al.*, 1978a,b, 1979; *Winckler*, 1980]. Generally, the signal to noise ratio of these artificial aurorae was low and imaging of the aurora was done from the ground.

In addition, space experiments in which electron beams were emitted are a conventional technique used to investigate natural electron beam processes. For example, electron beams have been used to trace magnetic fields to investigate the structure of the magnetosphere [e.g., *Winckler et al.*, 1989; *Hallinan et al.*, 1990], to probe the local electric fields [*Melzner et al.*, 1978; *Junginger et al.*, 1984], and to generate electromagnetic waves by beam modulation [*Burch et al.*, 1993].

In a more recent experiment, an electron accelerator the Space Experiments with Particle Accelerators (SEPAC) electron gun was included in the Atmospheric Laboratory for

Paper number 95JA01105.
0148-0227/95/95JA-01105$05.00

Applications and Science (ATLAS) 1 shuttle mission payload Space Transportation System 45 (STS-45), launched March 24, 1992 to study the interactions of artificial electron beams with the atmosphere and to create artificial auroras. Also included in the payload was an imager the Atmospheric Emissions Photometric Imaging experiment (AEPI) designed to image these artificial aurora for the first time from the same platform as the electron accelerator. The favorable viewing geometry from the same platform as the electron gun was expected to produce images with superior signal to noise ratios when compared to earlier combined rocket and ground-based experiments. During the STS 45 shuttle flight, controlled electron beam generation and high signal to noise ratio imaging of the resulting artificial aurora were accomplished successfully on several occasions [*Burch et al.*, 1993; *Mende et al.*, 1993]. The purpose of this paper is to further investigate the shape and evolution of artificial aurora generated during the ATLAS 1 shuttle mission.

SEPAC and AEPI Instrumentation and Preliminary Results

The SEPAC experiment on the ATLAS 1 mission was designed to accelerate electron beams up to energies of 6.25 keV with beam currents of up to 1.21 A. A previous flight of this experiment [*Obayashi et al.*, 1984] demonstrated that the spacecraft potential must be actively controlled to achieve such high beam energy and current. This was accomplished on the ATLAS 1 mission by (1) flying the shuttle, tail-first during the artificial aurora experiments in order to collect neutralizing plasma on the conducting engine farings, (2) including three additional conducting spheres in the shuttle cargo bay, and, (3) perhaps most importantly, releasing Xe^+ ions during the beam pulses to neutralize the charging effects of the significant electron beam current. Langmuir probes and other plasma instrumentation in the cargo bay indicated that these measures were effective, and controlled electron beams up to the highest energy were injected into the surrounding plasma [*Burch et al.*, 1993].

During the artificial aurora experiments, the SEPAC electron gun generated a 1-s pulse of 6.25 keV electrons with a beam current of 1.21 A. The delay between pulses was 10 s when operated manually (by the shuttle astronauts) and 15 s when operated automatically.

The AEPI experiment was designed to image artificial and natural auroras as well as atmospheric airglow [*Sandie et al.*, 1983]. The package consisted of two separate imagers with a shared video line. For the artificial aurora experiment, one imager observed in the visible continuum (white light) and the other imaged in a narrow (2.2 nm) bandwidth centered on the 427.8-nm N_2^+ first-negative band. The white light imager was operated at the standard TV frame rate (30 frames per second with a fixed 1/30 s integration), and the filtered imager made 1-s exposures every second. Both imagers had a field of view of about 16° by 20°. In order to observe the electron beam-induced auroras the AEPI instrument was pointed along the local magnetic field and in the direction toward Earth. Although the AEPI experiment had the capability of synchronizing with the SEPAC electron gun, the artificial aurora sequences discussed below were imaged without this synchronization.

Two separate artificial aurora sequences on two different shuttle orbits were imaged. During the first sequence, the SEPAC electron gun was pulsed at 10-s intervals, and only five artificial aurora "patches" were successfully imaged in white light. During the second sequence, the SEPAC electron gun was pulsed at 15-s intervals, and a total of 15 patches were imaged in both the narrow band filter and the white light. In these sequences on different orbits separated by about 3 hours, the shuttle was at about 300 km altitude, between 100° and 130° east longitude, and at about -56° latitude (the maximum southern latitude of the orbit). This placed the shuttle in the southern auroral zone (L shell between 4 and 6) and several AEPI images contained natural as well as artificial aurora [*Mende et al.*, 1993].

Preliminary results from the AEPI experiment suggested that the artificial aurora patches created by the SEPAC electron beam were the line-of-sight integral emission over distances from near the shuttle (essentially within the cargo bay) to ~190 km away (i.e., at altitudes of ~110 km above the Earth). As expected, the observations obtained with the white light imager were significantly different from those obtained by the 427.8-nm imager. These preliminary results are listed below [see *Mende et al.*, 1993].

From the 427.8-nm imager it was observed that

1. The artificial auroral patch was much larger in spatial extent than expected for emissions at 110 km altitude only (extending over several pixels instead of approximately 1 pixel).

2. The patch was much brighter than expected. On the basis of postflight intensity calibrations the video signal intensity peak was estimated to be equivalent to ~5 kR instead of 1.6 kR, the theoretically calculated value, derived from assuming that the interaction with the atmosphere takes place at 110 km altitude and the beam energy and atmospheric conversion efficiency are known.

3. The patch was complex, consisting of a more diffuse and somewhat asymmetric "head," a "tail," and a much smaller "spot" near the head but below the tail axis. The tail was pointed generally in the direction opposite the spacecraft motion.

4. There was no significant diffuse background glow around the observed patches.

From the white light imager it was observed that

1. The patch consisted of a head and tail, but the head appeared to be more symmetric than the head in the 427.8-nm images. A smaller spot near the head but below the tail axis was not nearly as evident as in the filtered images.

2. There was significant diffuse background glow permeating essentially the entire field of view of the imager during beam pulses. This background glow had a time profile which varied from pulse to pulse.

Some differences between the 427.8-nm and the white light observations were expected because

1. The integration time was different for the two imagers. The 427.8-nm images were 1-s exposures taken every second, whereas the white light images were taken at standard video frame rate (30 frames per second with a 1/30 s integration time). Since each electron beam pulse lasted only 1-s, the patches appeared generally on two consecutive filtered image frames and on about 29 white light image frames.

2. The emissions were from different source electrons. The production of the 427.8-nm N_2^+ first-negative band requires relatively high-energy (>20 eV) electrons. Therefore the 427.8-nm emission is the product of the energy deposition of energetic primary and the more energetic component of the

secondary electrons. In contrast, the white light imager was sensitive to the entire visible spectrum which contained lines and bands with energy thresholds of only a few eV. Some of these intense lines (such as the 557.7-nm O^1S line) are produced by low-energy electrons from secondary plasma processes.

3. The emissions had different lifetimes. The 427.8-nm N_2^+ first-negative band is an allowed transition with very short lifetime (<1 ms), and the emission is produced essentially instantaneously. In contrast, the white light images have strong contribution from the 557.7-nm O^1S auroral line which has a long (~0.7 s [*Vallance-Jones* , 1974]) lifetime. Therefore a time lag is expected in the emissions observed by the white light imager when compared with the 427.8-nm emissions observed by the filtered imager. This should produce a long exponential decay in the intensity of the white light emissions when compared to the 427.8-nm emissions. However, whether the emission lifetime is short or long should not affect the location of the peak emissions. The peak emissions should occur at the same point in the two images provided the parent state is produced rapidly by a short duration production function.

In this paper, we consider the shape and evolution of the auroral patches, separately as seen in 427.8 and in white light. We will investigate the preliminary results listed above in greater depth. While related to the shape and evolution, the absolute brightness of the 427.8-nm auroral patch is considered in detail elsewhere (T. Neubert et al., The SEPAC artificial aurora, submitted to *Geophysical Research Letters,* 1994).

We will first consider the white light images, investigating the diffuse background glow and the growth and structure of the tail of the auroral patch. Following this investigation, we will consider the filtered images, demonstrating that the overall shape of the head, tail, and small spot can be understood by accounting for emissions along a magnetic field line from near the shuttle to approximately 110 km altitude.

White Light Observations

Diffuse Background Glow

Plate 1 shows a sequence of eight white light images of one of the artificial auroral patches. Each image is a small part (approximately 3° x 6°) of the full field of view of the imager. The frame numbers are shown above each image. The SEPAC beam pulse started at frame number 14, and selected frames are shown from approximately the first third of the 30 frames obtained during the 1-s beam pulse. A scale in milliradians is shown next to frame number 15, and a corresponding scale in kilometers at 100 km altitude (200 km range from the shuttle) is shown next to frame number 14. In these and subsequent images the instrument is looking almost exactly in the nadir direction (also almost exactly along the magnetic field), south is up, east is to the left, and the shuttle velocity vector is nearly horizontal and also directed to the left.

Three features are evident in the temporal sequence in Plate 1. First, there is a diffuse glow filling nearly the entire image that increases in intensity during the beam pulse. Second, the artificial auroral patch itself is relatively diffuse and also increases in apparent intensity. Third, the patch has a tail that grows in apparent length and intensity with time (compare the first and last frames). The tail extends in the direction opposite the spacecraft velocity vector.

The upper panel of Figure 1 shows the time profile of the white light intensity during another beam pulse. The duration of the 1-s beam pulse is indicated by the black line between the two panels. The solid curve in the upper panel is the peak intensity, defined as the highest intensity pixel in the patch. The dotted curve is identified as the near background. The near background intensity was determined by averaging over many pixels at a location along the spacecraft velocity vector ahead of the auroral patch (i.e., the upstream side of the patch, in the opposite direction of the tail). Electrons in the narrow beam do not reach this part of the image. The dashed line is the peak intensity minus the near background intensity. Once the background is removed, the peak intensity of the auroral patch has a sharp rise at the start of the beam pulse, is remarkably flat over the 1-s pulse, and has a somewhat more gradual decay at the end of the pulse. This same procedure for removing the background was done for all artificial auroral patch sequences (not shown). When the variable background was removed, all white light images of the artificial auroral patches had nearly the same peak profile and absolute intensity as the one illustrated in Figure 1. This similarity is attributed to the repeatable beam voltage and current of the SEPAC experiment and also apparently to the repeatable beam-plasma interactions in the upper atmosphere. Because the peak intensities of the auroral patches were so similar after background was removed, we will use different auroral patches throughout this paper interchangeably to emphasize features of their shape and evolution.

The bottom panel shows the profile of the current from one of several Langmuir probes that were part of the SEPAC experiment. This probe was located in the shuttle cargo bay. The current profile approximately follows the total and near background intensities in the top panel. In particular, there is a peak in the current in the second half of the beam pulse and a much more gradual decay in the current at the end of the pulse. Other Langmuir probe current profiles from other beam pulses are not correlated as well as suggested in the profiles of Figure 1. One possible reason for this lack of correlation is that the Langmuir probe was not operated at saturation and changes in the local spacecraft potential could also cause current changes. Although a separate floating probe usually indicated no significant change in the spacecraft potential, the variability in the Langmuir probe current from pulse to pulse indicates that the correlation depicted in Figure 1 is either fortuitous or the Langmuir probe measurements are sometimes unreliable. The important results from Plate 1 and Figures 1 are that the intense, diffuse, and highly variable background seen during beam pulses is probably due to emissions essentially in the cargo bay of the shuttle. Because no similar background was observed in the filtered images [*Mende et al.*, 1993], the background in the white light images is probably due to relatively low-energy electrons (~few eV). If the electron energy were greater than about 20 eV, then they would have produced background emissions in the filtered images. There is a strong possibility that few eV electrons are responsible for the variable low-energy electron background detected by the Langmuir probes in the cargo bay. One indication of the close proximity of the low-energy electrons to the shuttle is that the background emissions fill the field of view of the white light imager. However, because the emitters were not moving with the shuttle, their velocity in the shuttle frame of

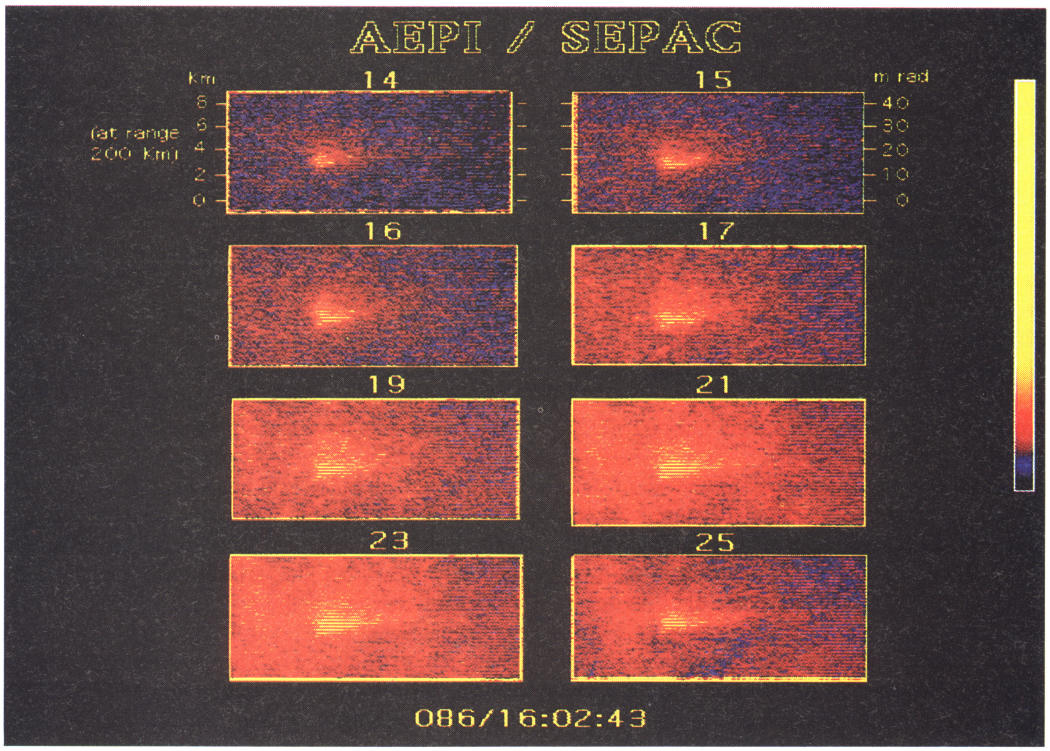

Plate 1. White light images of one artificial auroral patch from individual video frames. The frame number is shown above each 1/30-s image and a scale size in milliradians and kilometers is shown on the top right and left images, respectively. The 1-s electron beam pulse started at frame number 14. During the beam pulse, a bright, diffuse background develops. Also, a tail grows on the artificial auroral patch.

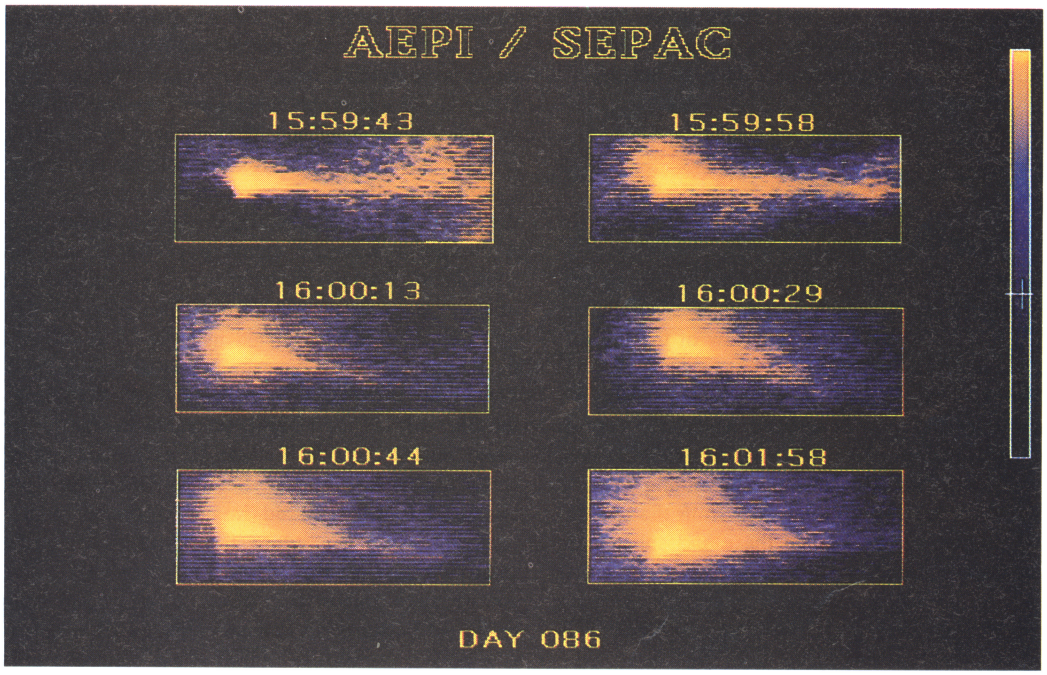

Plate 2. Six composite white light images of artificial auroral patches. These composite images were produced by summing approximately 30 individual white light images with background removal. Each image shows a relatively diffuse head and a tail. The head is asymmetric, being brighter and more diffuse in the half plane above the tail axis. The tail extends in the general direction opposite the spacecraft motion but deviates from this direction by more than 10° for the three patches starting at 1600:13 UT.

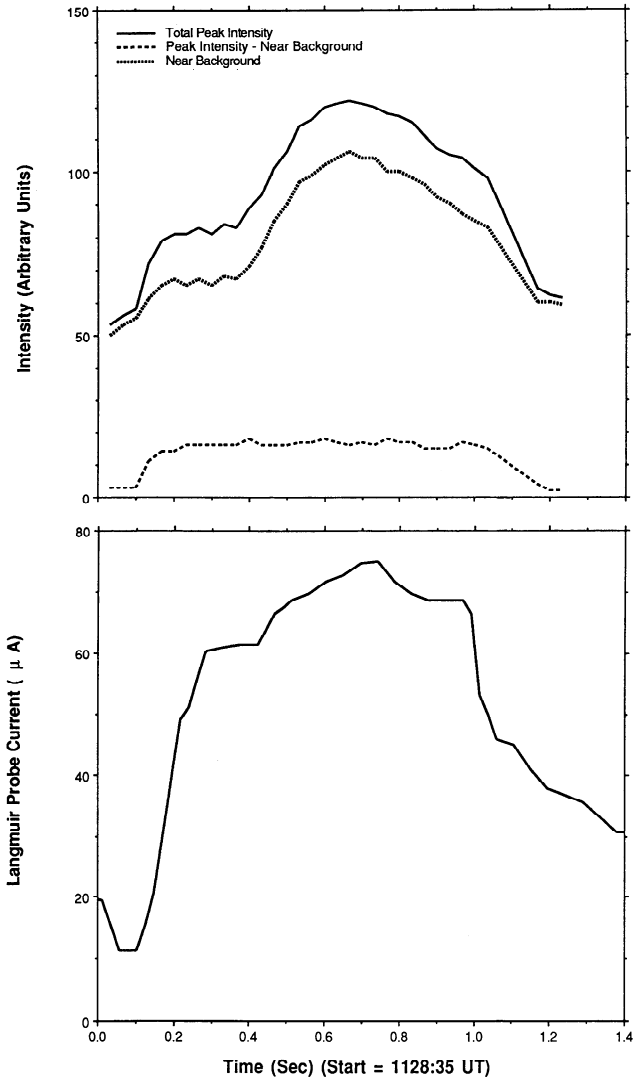

Figure 1. (top) The total peak intensity, background intensity, and peak intensity with background removed profiles for one of the artificial aurora patches. (bottom) The Langmuir probe current from a probe in the shuttle bay. The black bar between top and bottom panels represents the beam pulse period. The background intensity increases during the beam pulse as does the Langmuir probe current. When the background is removed, the peak intensity rises sharply when the beam pulse begins, is very flat during the 1-s beam pulse, and decays somewhat more slowly at the end of the beam pulse.

reference was 7.8 km/s and their close proximity to the shuttle would have resulted in a large apparent motion sweeping them rapidly out of the field of view before they had a chance to emit light. Therefore in order to be readily visible, the longer lifetime white light emissions responsible for the background had to be produced in the atmospheric gases which are entrapped in the cargo bay and comoving with the shuttle.

Shape of the Auroral Patch in White Light

Composite images were produced by summing the nearly 30 video frames obtained in a 1-s beam pulse after the diffuse background was removed in the manner discussed in connection with Figure 1. The combination of almost 30 frames with background removed produces a very high signal to noise ratio (~30 to 1). For comparison, previous rocket experiments of artificial aurora had signal to noise ratios of only ~4 to 1 [e.g., *O'Neil et al.*, 1979]. Figure 2 shows one of these composite images in a three-dimensional perspective plot. The high signal to noise ratio is evident from this presentation. The most striking feature is the long tail. The "head" of the patch shows a slight asymmetry in the up-down (south-north) direction. As discussed below, this is probably related to the curvature of the magnetic field and is much more apparent in the filtered images.

Plate 2 shows white light composite images of six of the auroral patches in a time sequence from 1559:43 to 1601:58. The angular size of each image is about 2° x 5°. Each image in Plate 2 shows an artificial auroral patch composed of a somewhat diffuse head and a long (several kilometers at 110 km altitude) tail. Like the contour plot representation of the image in Figure 2, the head of the patches in Plate 2 is often more diffuse in the half plane above the tail axis (in the more southerly direction) than in the half plane below the axis. The spacecraft velocity vector is directed nearly horizontal and to the left, and the tail is directed approximately opposite this direction. Although the spacecraft velocity changes from slightly downward in the image to slightly upward and back again during the six beam pulses, the tail deviates much more strongly (over 10°) from the velocity direction for the three images starting at 1600:13. There may be some evidence for a small spot near the head of the patches in the half plane below the tail axis (see for example the patch at 1601:58 UT). This spot is much more apparent in the filtered images (see below and *Mende et al.* [1993]).

The appearance of a long tail is not surprising in the white light images because the spectral bandwidth of the image (from 430 to 850 nm but containing a notch filter at 762 nm to suppress airglow) contains several prominent lines that have very long decay times [*Mende et al.*, 1993]. Therefore the tail opposite the spacecraft velocity vector could be simply the decay of long-lived emissions (such as the 557.7-nm O^1S line with a decay time of 0.7 s) that have been excited slightly earlier by the beam. These long-lived emissions appear downstream from the head of the artificial auroral patch and at a lower intensity because of the 7.8 km/s motion of the shuttle and the decay in the emissions, respectively. The apparent deviation of the tail direction from the direction exactly opposite to the velocity vector is puzzling, and no satisfactory explanation has been provided yet.

Growth of the Tail and Altitude of the White Light Emissions

As discussed in connection with Plate 1, the tail of the artificial aurora is observed to grow during the 1-s beam pulse. To illustrate this growth, the intensity of an auroral patch measured by the white light imager was integrated over the direction perpendicular to the tail axis of the patch to produce a one-dimensional intensity profile along the tail axis. The background was removed from each of the 30 profiles obtained during a beam pulse, and the amplitude of each profile was normalized between zero and one with one being the peak amplitude. The one-dimensional normalized intensity profiles for one of the artificial auroral patches were combined to produce the relief plot shown in the top panel of Figure 3. In

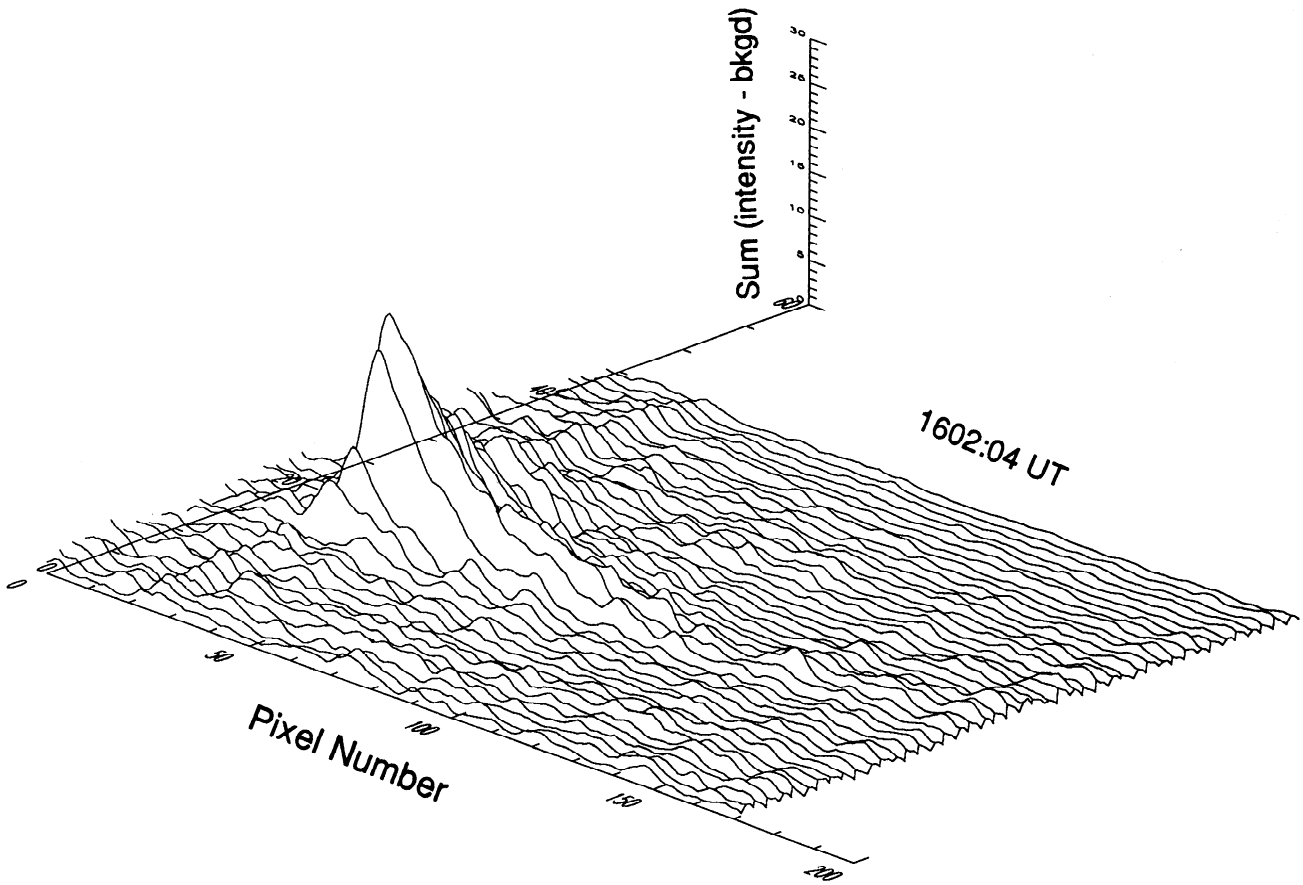

Figure 2. Intensity versus x and y position of a composite white light image. The excellent (30 to 1) signal to noise ratio is obtained by summing and averaging approximately 30 individual white light images with background removal. The most striking feature of this white light image is the long tail. Also, some asymmetry in the south-north (y) direction is seen in head of the spot.

this Figure 3, the x axis is the pixel number increasing with distance down the tail axis (downstream from the peak), the y axis is time starting at the beam pulse, and the z axis is the normalized intensity. The time profile for the location 23 pixels down the tail from the peak intensity is shown in the bottom panel of Figure 3. This time profile clearly shows that the intensity at this location was low during about the first 0.15 s of the 1- s beam pulse but increased to reach an approximate plateau after the first half of the pulse.

In Figure 3, it is apparent that some tail emissions appeared essentially instantaneously (within one TV field) since the intensity at 23 pixels down tail from the peak is not zero (0.4) at the beginning of the beam pulse. However, the later increase in the intensity in the bottom panel indicates that additional tail emissions appear at this location somewhat after the beginning of the beam pulse. It is this later increase in intensity that is used to determine the distance from the shuttle to the tail of the emissions.

The later intensity increase in the tail is likely the combination of two effects. First, there is the intrinsic risetime of the intensity of the emissions. Independent of the decay time of the emissions, if the rise in intensity is slow, then the later intensity increase will appear down tail from the peak intensity because the shuttle motion (moving the beam in the direction of the velocity vector) is fast compared to the risetime. An example would be emissions that result from a cloud of secondary electrons generated at some later time than the initial beam electrons. Second, there is the initial growth of the tail in length after onset of the beam. As the shuttle moves, the peak intensity remains fixed relative to the shuttle but moves in the atmosphere with the shuttle speed, resulting in a tail that appears to grow in length. Since the intensity profile of the tail is a decreasing exponential, a growth in length at a point on the tail appears as a growth in intensity.

The exponential decay in the emission intensity that leads to the growth of the tail is illustrated on Figure 4. The frame of reference for Figure 4 is the stationary atmosphere below the shuttle. Initially, the beam produces a single small spot at full strength (frame 1). During Frame 2 the beam hits the adjacent region (because of the shuttle motion), but some residual intensity is emitted from the previous region due to the decay of the emissions. During frame 3, there will be three regions illuminated forming the beginning of an exponential tail. Since the peak intensity moves with the shuttle, the tail appears to grow in length in the atmosphere. Alternately, a region some distance from the brightest spot would appear to grow in intensity after a few frames' delay.

In Figure 4, it is assumed that the risetime of the emission intensity is fast compared to the time the shuttle moves a noticeable distance. If the risetime is slow, then the time required for the tail to grow to the location 23 pixels from the peak intensity in Figure 3 is the combination of the intrinsic risetime of the emission intensity and the time required for the shuttle to move the distance between the point of the beam

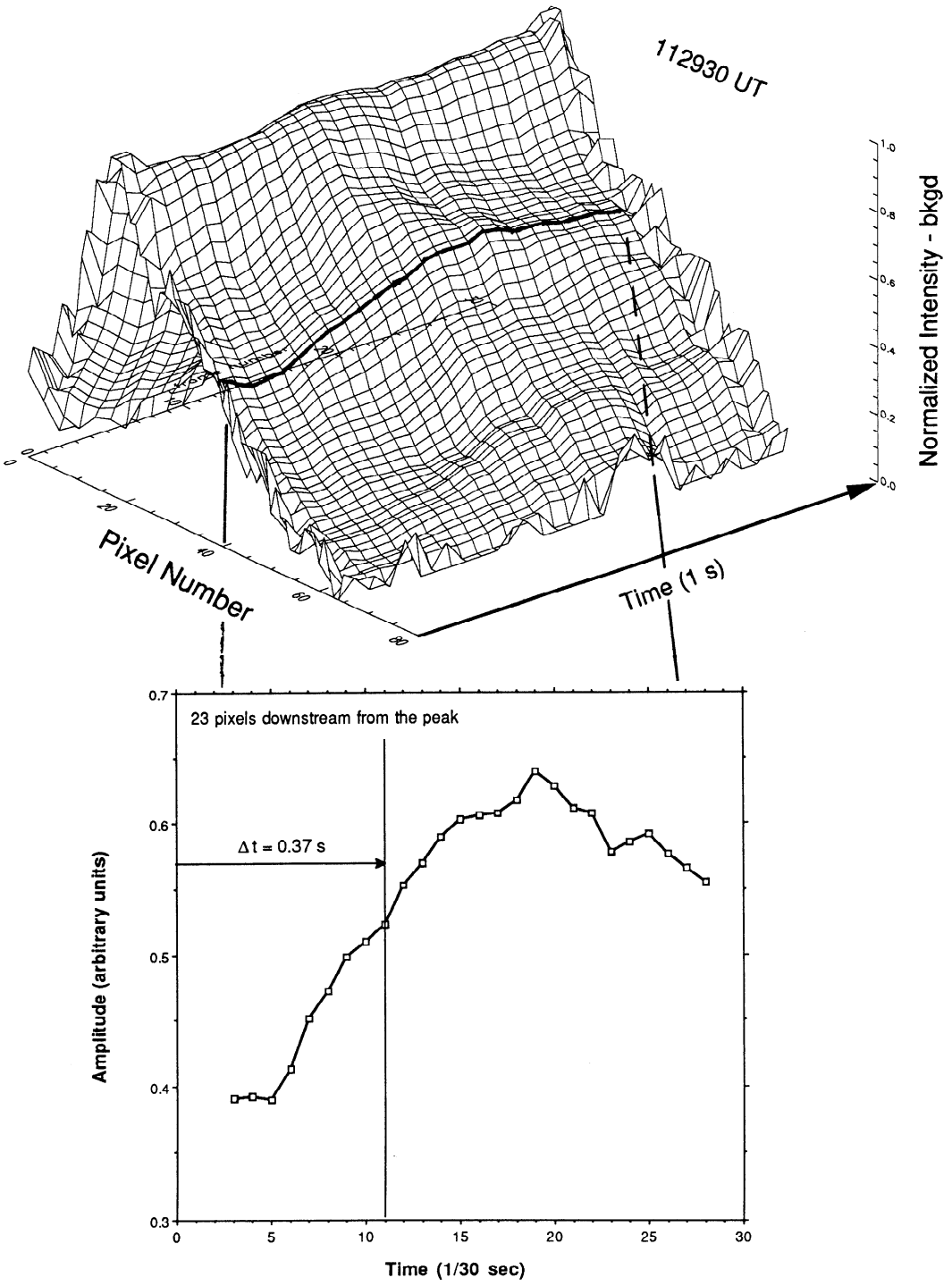

Figure 3. (top) One-dimensional white light intensity profiles along the tail axis for a beam pulse. The x axis is pixel number along the tail axis, the y axis is time in units of 1/30 s, and the z axis is normalized intensity (normalized between 0 and 1) with background subtraction. (bottom) The time history of the normalized intensity 23 pixels down the tail of the patch from the peak intensity. Note that the initial intensity immediately after the start of the beam is at 0.4. The initial rise to this level takes place within first TV frame. During the beam pulse, the tail grows and, after about 1/3 s, encompasses the location 23 pixels downstream (down the tail) from the peak intensity.

onset and pixel 23. Since the intrinsic rise time of the emission intensity is not known a priori in this case, the observations in Figure 3 cannot be used to determine the distance from the orbiter to the tail emissions.

However, there is evidence that at least some of the emissions in the white light imager have a very rapid rise time and a relatively long decay time as illustrated in Figure 4. At the beginning of the beam pulse, the intensity in the tail is

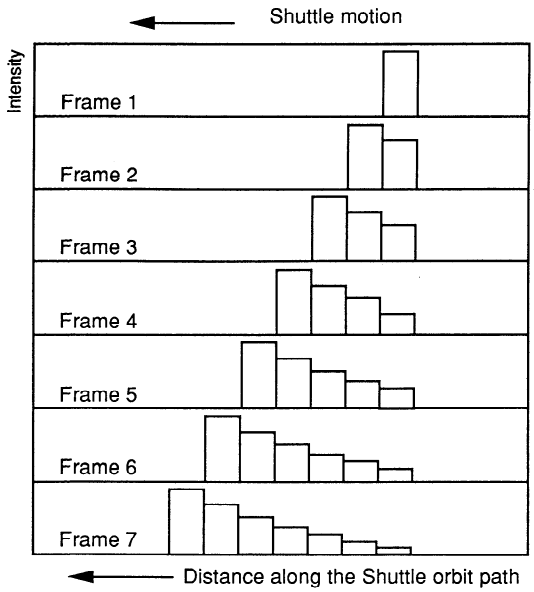

Figure 4. Schematic illustration of the growth of the white light tail assuming a rapid risetime for the emissions and a long decay time. The frame of reference is the stationary atmosphere below the shuttle. In image frame 1, the beam illuminates a small patch. In frame 2, the beam illuminates an adjacent patch because of the shuttle motion, but decaying emissions from the patch in frame 1 are also seen. By frame 3, the development of an exponential tail is seen.

not zero (see the lower panel of Figure 3). This indicates that at least some of the emissions in the tail have a very rapid risetime compared to the time taken by the shuttle to move the distance of one pixel. Furthermore, the wavelength range includes significant contributions from the 557.7-nm O^1S line with a decay time of 0.74 s. This time is very long compared to the shuttle motion.

Considering this evidence, it is assumed here that the emissions in the tail have a very rapid rise time but a long decay time. Therefore, the growth time of the tail to a certain distance is simply related to the distance the shuttle moves in that time (see Figure 4). The conversion from growth time to distance is then

$$Y = \Delta t \, V_{SC}, \tag{1}$$

where Δt is the time for the tail to grow to a length Y and V_{SC} is the shuttle orbital velocity (7.8 km/s in the direction opposite the tail axis). From the angular extent of the tail in the imager, ϑ, the distance from the shuttle to the tail of the auroral patch is then determined from

$$D = Y / \tan(\vartheta) \tag{2}$$

where D is the distance from the shuttle to the tail emissions and, Y is the size of the tail given by (1).

There are at least two tail components with very different growth times in Figure 3. The first component has a nearly instantaneous growth time and is responsible for the increase in intensity from 0 to 0.4 on the arbitrary intensity scale in the bottom panel. These emissions must be very near the shuttle because they appear essentially instantaneously in the tail. (Note however, that they are not associated with the background emissions in the last section since the background emissions were removed in Figure 3). The second tail component appears at a somewhat later time and is responsible for the increase in the intensity of the emissions from 0.4 to 0.6 on the arbitrary intensity scale. Using Figure 3, we determine that the growth time for these later tail emissions is about 0.37 s (11 frames after the beam pulse begins), and Y = 2.89 km from (1). In the 0.37 s, the slower growing part of the tail increased by a total of 23 pixels from the peak. One pixel is 142 arc sec so 23 pixels subtend an angle ϑ=0.91°. Therefore, using these numbers and (2), the distance from the shuttle to the slower growing part of the tail in Figure 3 was D = 180 ± 35 km. In other words, this component of the tail emissions originated at an altitude of about 120 km, given that the shuttle altitude was 300 km. The primary uncertainty in this distance measurement is in Δt, the growth time 23 pixels down tail from the peak intensity (see Figure 3).

The white light observations confirm that a component of the tail is formed at 120 ± 35 km altitude. These observations also suggest that there is a second component very near the shuttle. Model predictions and filtered images of the artificial aurora also suggest that there are emissions at different altitudes.

The volume emission rate for 427.8 nm as a function of altitude for the 6.25 keV electron beam was modeled by *Mende et al.* [1993]. These model predictions from *Mende et al.* are shown in Figure 5. The model assumes that the imager is looking directly along the axis of a cylinder containing the magnetic field and a 10-m-wide electron beam. Emissions (at 427.8 nm) generated by excitation of N_2^+ ions in a simple model atmosphere [*Rees et al.*, 1976] are collected by this imager. These emissions are the sum of near-field emissions not subject to the inverse square law and far-field emissions that are subject to the inverse square law. A 10-m-wide electron beam will become a point source in the image within a few

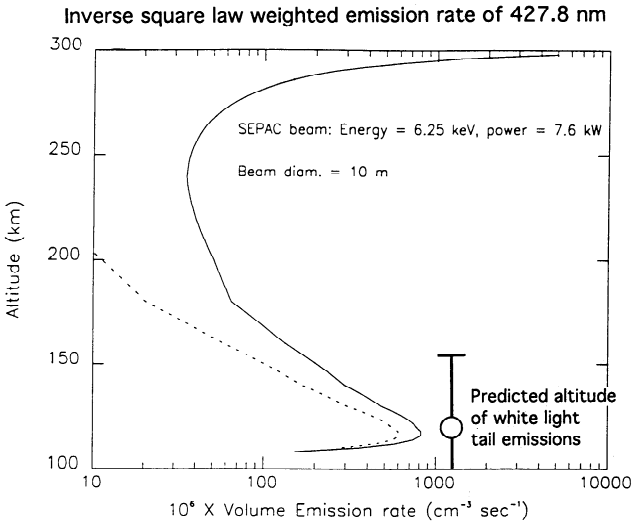

Figure 5. Apparent volume emission rate profiles from *Mende et al.* [1993]. The dashed line shows the emission rate with no inverse square law, while the solid line shows the emission rates when the inverse square law is taken into account. The imager observes emissions from all along the magnetic field from 300 km to 110 km altitude. The altitude of the white light tail emissions described in Plate 2 is shown.

kilometers from the shuttle because at this distance the angular resolution of the camera is no longer adequate to resolve the beam. Thus the far-field emissions originating from a distance of 10 km or more from the shuttle (shuttle altitude= 290 km) will be subject to the inverse square law. Under these assumptions, the volume emission rate as a function of altitude without accounting for the inverse square law is shown by the dashed line in Figure 5 and the emission rate accounting for the inverse square law is shown by the solid line. Also shown in the Figure 5 is the altitude of the white light emissions in the tail computed from the tail growth. Although these emissions are primarily from line emissions other than 427.8 nm, they should have a similar height profile. Thus the agreement between this simplistic model using a straight magnetic field and model atmosphere and the observed white light emissions in the tail is quite good despite the uncertainties in the measurement.

Monochromatic Observations.

Unfortunately, the filtered images were averaged over 1-s (commensurate with the 1-s beam pulse). Thus, even though a tail was observed in the filtered images [e.g., *Mende et al.*, 1993], no tail growth could be observed and a similar calculation of the distance to the 427.8-nm tail emissions could not be done. However, the relative distance to parts of the 427.8-nm auroral patches can be estimated from the fact that the magnetic field line in the images is not straight. Because the field line is not straight, emissions coming from different altitudes, as suggested by the model results in Figure 5, will have an angular offset in the image. For example, an initial estimate of the angular offset of emissions near the shuttle and at 110 km altitude was about 8 milliradians, corresponding to a 1.7-km offset at 110 km altitude [*Mende et al.*, 1993]. We investigate this possible offset further by using a dipole magnetic field model centered on the south magnetic pole to determine the bend in the magnetic field from the 300-km shuttle altitude to the 110-km base of the emissions estimated from the model results in Figure 5. Figure 6 shows the results of this investigation.

The upper panel in Figure 6 is a schematic of the orientation of the magnetic field, the orientation of the imager, and the direction tangent to the magnetic field at the shuttle altitude. The imager views almost exactly along the magnetic field. If the magnetic field through the center of the imager were straight, it would appear as a point in the image. However, the magnetic field line is curved and will therefore intersect the 110 km altitude at a point displaced from the tangent to the magnetic field at the shuttle altitude. Since the AEPI observations occurred in the southern hemisphere near the Australian longitude sector (100-130° E longitude), the magnetic field is pointing northward and westward in the geographic reference. On account of the curvature of this field line, the direction antiparallel along the magnetic field from the shuttle altitude to 110 km (that is, the direction the beam electrons will take) will be displaced in the image slightly northward and slightly westward from the local tangent direction. The northward displacement is illustrated in the top panel of Figure 6 by the line labeled **B** which terminates at 110 km altitude.

The lower panel of Figure 6 shows an enlargement of a filtered (427.8 nm) image of an auroral patch. The head, tail, and small spot below the tail axis of the patch are shown as is

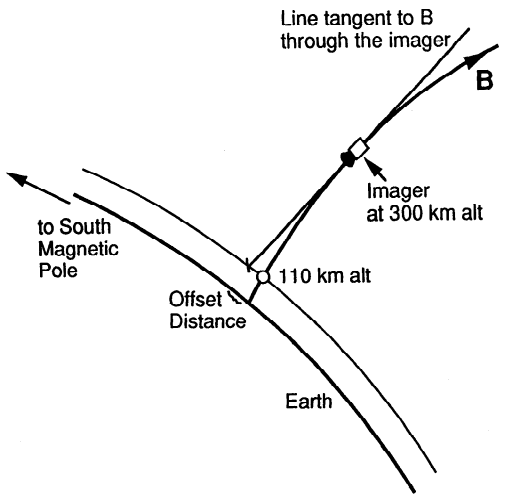

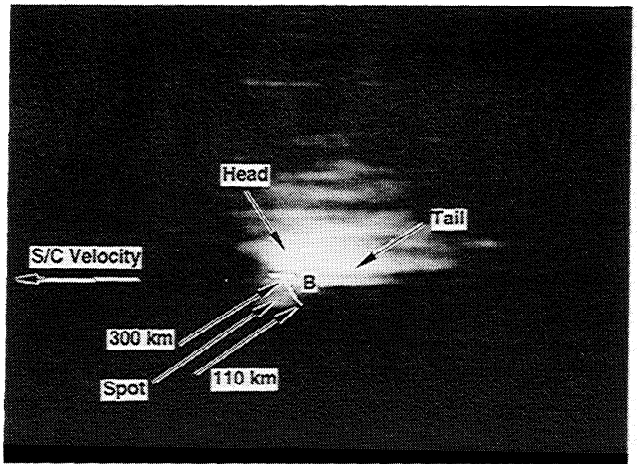

Figure 6. (top) A schematic of the imager view along the magnetic field and the magnetic field curvature, resulting in an offset approximately in the vertical direction between the magnetic field at 300 km and the same field line at 110 km altitude. (bottom) A filtered (427.8 nm) image of one of the auroral patches showing the head, tail, and small spot below the tail axis. The trace of the magnetic field line from 300 km to 110 km altitude indicates that the approximate vertical direction in the image is equivalent to distance along the magnetic field. Because of the spacecraft velocity, the horizontal direction is also a time variant. Therefore the emissions in the head occurred nearer the shuttle than the tail emissions, and the emissions in the small spot probably occurred at the lowest altitudes. Because these emissions occur to the left of the head and tail emissions (that is, earlier in time), the risetime for the relatively nearby head and tail emissions must be longer than the risetime for the spot emissions.

the direction of the spacecraft velocity. Also shown by the short dash labeled "300 km" is the location of the tangent field line that runs through the imager center field of view. Note that the trace of the magnetic field line from 300 km to 110 km in the image has been offset from the head of the artificial auroral patch somewhat for clarity.

Due to the curvature of the magnetic field in the image, the location of the tangent to the field line through the imager and

the intersection of the field line itself with the atmosphere at 110 km altitude are offset by about 1.2 km (at 110 km altitude). This offset is similar to the 1.7-km offset estimated by *Mende et al.* [1993]. Therefore emissions from the electron beam that occur along the field line should appear to come from different near-vertical directions in the image. Furthermore, the motion of the shuttle during the 1-s exposure will cause emissions nearer the shuttle to have a larger tails (displaced opposite the spacecraft velocity) compared to emissions farther from the shuttle.

Because of the magnetic field curvature and the shuttle motion, the horizontal direction in Figure 6 is equated with time, while the vertical direction (bottom to top along the direction of the magnetic field line) is equated with altitude. Therefore it is apparent that the head of the patch and indeed all the emissions in the half plane above the tail axis occur close to the spacecraft (300 km altitude), while the tail occurs somewhat later in time (due to growth of emissions in the tail) and at a somewhat lower altitude. However, it is not apparent how the small spot below the tail axis fits this altitude/time interpretation. This spot must occur at the lowest altitude because it is farthest offset from the head and tail in the vertical direction. But the fact that it is not along the magnetic field from the head indicates that it occurs earlier in time than the emissions in the head. Since there is negligible propagation time from 300 to 110 km altitude for 6.25 keV electrons, the fact that the small spot occurs earlier in time from the emissions in the head and tail indicates that the emissions closer to the shuttle occur later on account of having a longer risetime than the emissions at the lowest altitudes.

This interpretation is consistent with the observation of a tail in the 427.8-nm filtered images. This tail was unexpected [*Mende et al.*, 1993] because emissions at this wavelength are prompt (<1 ms). Therefore the tail in 427.8-nm images cannot be due to decay of long-lived emissions as is possible in the white light images. Instead, there must also be 427.8-nm emissions that are excited by mechanisms that are active even after the electron beam has moved away due to the shuttle motion.

Discussion

In this paper, we have considered the shape and evolution of artificial aurora patches created by injection of a 6.25 keV 1.21 A electron beam into the upper atmosphere. White light and filtered images must be considered separately because, even though the artificial auroral patches are somewhat similar in that they consist of a head and tail (compare Plate 1 and Figure 6), the processes creating the emissions seen by the two imagers are quite different. One of the most striking examples of this difference is that the white light images of artificial aurora show a bright, variable, and diffuse background during the 1-s beam pulses (Plate 1), while the filtered images do not (Figure 6). Low-energy electrons essentially in the shuttle bay were detected in conjunction with this background in the white light imager (Figure 1), and these electrons are apparently responsible for the background emissions. Because no similar emissions were seen in filtered (427.8-nm) images (see Figure 6 and *Mende et al.*. [1993]), the background was probably generated by emissions with electron excitation thresholds on the order of a few eV, that is, lower than the ~20 eV threshold for 427.8-nm N_2^+ emissions. These low-energy electrons must be very close to the shuttle (essentially in the cargo bay) because the emissions fill the field of view of the imager. However, it would be expected that the intensity of such emissions would be very low unless they are comoving or trapped in the shuttle bay, because atoms in long lifetime excited states would be swept out of the field of view prior to emitting.

When the background is removed, the total intensity and time history of the peak of the emissions in the white light camera are very similar for all the artificial aurora patches. They all show a relatively rapid rise at the beginning of the beam pulse, a very flat intensity profile during the pulse, and a somewhat more gradual decay at the end of the pulse (see the dashed line in Figure 1). The gradual decay is likely due to relatively long-lived emissions such as those at 557.7 nm.

The patches observed in white light have a relatively diffuse head and a long tail (Figures 2 and Plate 2). The tail is directed approximately opposite the spacecraft velocity vector but does show deviations of the order of 10° from this direction (Plate 2). The tail in the white light image is not surprising considering that at least some of the emissions are long lived (up to 0.74 s for the 557.7-nm line) and, combined with the shuttle motion during the 1-s beam pulse, this decay will form a tail. Components of the tail are observed to grow with different times during the 1-s beam pulse (Figure 3). One component grows essentially instantaneously while a second component grows more slowly. Assuming that the risetimes of both components of the tail emissions are rapid, the distance from the shuttle to the tail emissions was estimated. The component that grows nearly instantaneously must be very close to the shuttle, while the more slowly growing component was estimated to be about 180 km from the shuttle (at 120 km altitude).

The filtered (427.8 nm) images of the artificial aurora patches have a complex structure with a somewhat diffuse head, a tail in the general direction opposite the spacecraft motion, and a somewhat fainter spot near the head in the half plane below the tail axis (Figures 6). The presence of a tail in the filtered images was unexpected because these emissions are prompt (<1 ms). It was not possible to observe tail growth in the filtered images because they were 1-s exposures of the 1-s beam pulse. However, the curvature of the magnetic field and the motion of the shuttle during the 1-s exposure allow an estimate of the relative altitude of the component emissions of the filtered images. In the filtered image in Figure 6, the motion of the spacecraft allows us to equate the horizontal direction with time, while the displacement of the magnetic field line allows us to equate the direction along this displacement (approximately 45° from the image vertical) with distance from the shuttle.

With these definitions, it is apparent that the relatively diffuse head of the patch occurs close to the shuttle, while the tail occurs somewhat farther away. A puzzling aspect of the patch is the position of the relatively small spot near the head which we identify as the classical distant artificial aurora produced deepest in the atmosphere by its location below the tail axis. If the head, tail, and small spot emissions all had the same fast risetime, then their origin should be seen to lie along one line that follows the trace of the magnetic field line in Figure 6. Because the artificial auroral spot is to the left of the magnetic field line relative to the head and tail emissions, it must have occurred earlier in time than the head and tail emissions. Since there is negligible delay in beam

propagation time from 300 to 110 km altitude, the spot emissions must have had a shorter risetime than those in the head and tail. Figure 7 illustrates this point. Viewing the 427.8-nm emissions from a stationary orbiter is equivalent to introducing a "wind" that will cause the emissions to spread with time. In the image, the horizontal axis will be time and, if the beam is also displaced in the vertical direction in the image due to displacement of the magnetic field line (as in the image in Figure 6), then the vertical axis will be distance along the magnetic field. If there are now two sets of 427.8 emissions, one located at 110 km altitude occurring promptly with a very short risetime and a second located nearer the shuttle with a somewhat longer risetime (see Figures 5 and 7), then the resulting artificial auroral patch will have a shape similar to that in Figure 6, with the longer risetime emissions forming the rather diffuse head and extended tail.

In summary, the 427.8-nm emissions show three anomalous features: (1) there appears to be a bright region produced by the electron beam which is much closer to the orbiter than the artificial aurora spot produced at the conventional 100 - 120 km altitude; (2) this bright region has a decay time which must be in the range between 1 ms and to 1-s depending on the distance between the bright region and the orbiter; (3) there is a finite rise time associated with this emission. All the above properties but especially the last one involve some plasma process (not identified here) other than simple auroral electron excitation and decay of atomic and molecular states. The processes responsible for producing these effects might be the same as those observed in connection with rocket experiments in which prompt electron "echoes" were observed in the vicinity of the electron emitter. These energetic electrons were detected in the vicinity of the spacecraft, and they had a surprisingly long time decay of several tens of ms [*Wilhelm et al.*, 1985]. Such electron fluxes could have produce the 427.8-nm signatures observed in the vicinity of the field line containing the electron beam.

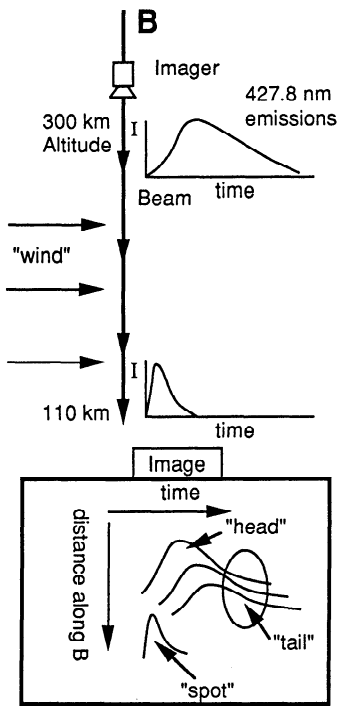

Figure 7. Schematic of the explanation of the structure of the artificial aurora patch. The imager moving at the spacecraft velocity is equivalent to an upper atmospheric wind blowing past a stationary imager. The imager views down along the magnetic field which curves in the third dimension. Because of the curvature of the magnetic field, the vertical direction in the image is equivalent to distance along the magnetic field. Because of the wind, the horizontal direction is time. Nearby emissions have a longer risetime, so they are observed at a later time than the emissions at 110 km altitude, which have a very short risetime. Tail emissions occur at intermediate altitudes.

It may appear that this interpretation of the filtered image is inconsistent with the calculation of the distance to the tail emissions in the white light image in Figure 3. In this calculation we assumed that the emission producing the white light tail is the result of a prompt production process which has no significant risetime. In view of the above discussion of the filtered image, it is possible that processes within the wavelength range of the white light imager do have a nonnegligible risetime. A slower risetime for the emissions in the tail will affect the estimate of the distance to the tail from the observations in Figure 3. If part of the time required to observe the tail growth to a certain distance from the peak of the emissions is the risetime of the emissions, then the actual Δt in (1) would be shorter and the size (Y in (1)) would be smaller. Since this shorter distance still subtends the same angle in the image, then from (2), it must occur closer to the spacecraft. As a quantitative example, if the risetime of the emissions within the wavelength range of the white light imager accounts for half of the Δt in Figure 3, then the white light tail emissions do not come from 120±35 km as estimated in Figure 3. Rather they come from about 210 km altitude (a factor of 2 closer to the shuttle).

The joint AEPI/SEPAC experiment has paved the way for producing large electron beams suitable for probing the atmosphere and the magnetosphere. It was demonstrated that beams can be ejected from a large spacecraft and that the optical signature of these beams, the artificial aurora, can be detected. However, we have learned that there are unanticipated features of the emissions produced by such beams which have to be taken into account for the successful performance of such electron beam experiments relying on optical detection: (1) There is considerable luminosity which is built up in the close vicinity of the orbiter and which is carried by the orbiter's trapped atmosphere; (2) in prompt emissions such as 427.8, there are substantial near field (several kilometers) components of the beam-induced optical emission, some of which, have a risetime and decay time probably associated with the generation process of the hot electron plasma; (3) the artificial aurora patch in the lower atmosphere can be spatially separated from the near-field emissions because of the curvature of the magnetic field; (4) most of the observed long-life time emissions are produced in the lower atmosphere (i.e., the classical artificial aurora) because the near-field emissions are not seen having been left behind by the fast moving spacecraft.

The observation of the relatively slow risetime and decay time of the 427.8-nm emission suggests that the same thing might occur in natural auroras and the models, which assume that the auroral electron beam interaction and subsequent production of secondaries are quasi-instantaneous, might be wrong. There may well be a hot electron population on auroral field lines with significant properties influencing the aurora besides their relatively slow production and decay rate.

Acknowledgments. Research at Lockheed was funded by NASA contract NAS8-32579. J. Burch was the PI for the SEPAC experiment, and N. Kawashima provided the Langmuir probe data.

The Editor thanks M.J. Rycroft and R.J. Nemzek for their assistance in evaluating this paper.

References

Burch, J. L., S. B. Mende, N. Kawashima, W. T. Roberts, W. W. L. Taylor, T. Neubert, W. C. Gibson, J. A. Marshall, and G. R. Swenson, Artificial auroras in the upper atmosphere, 1, Electron beam injections, *Geophys. Res. Lett., 20*, 491, 1993.

Davis, T. N., T. J. Hallinan, G. D. Mead, J. M. Mead, M. C. Trichel, and W. N. Hess, Artificial aurora experiment: Ground-based optical observations, *J. Geophys. Res., 76*, 6082, 1971.

Hallinan, T. J., H. C. Stenbaek-Nielsen, and J. R. Winckler, The Echo 4 electron beam experiment: Television observations of artificial auroral streaks indicating strong beam interactions in the high-latitude magnetosphere, *J. Geophys. Res., 83*, 3263, 1978.

Hallinan, T., J., J. R. Winckler, P. Malcolm, H. C. Stenbaek-Nielsen, and J. Baldridge, Conjugate echoes of artificially injected electron beams detected optically by means of new image processing, *J. Geophys. Res., 95*, 6519, 1990.

Hess, W. N., M. C. Trichel, T. N. Davis, W. C. Beggs, G. E. Kraft, E. Sassinopoulos, and E. J. R. Maier, Artificial auroral experiment: Experiment and principal results, *J. Geophys. Res., 76*, 6067, 1971.

Junginger, H., G. Geiger, G. Haerendel, F. Melzner, E. Amata, and B. Higel, A statistical study of dayside magnetospheric electric field fluctuations with periods between 150 and 600 s, *J. Geophys. Res., 89*, 5495, 1984.

Melzner, F., G. Melzner, and D. Antrack, The GEOS electron beam experiment S 329, *Space Sci. Instrum., 4*, 45, 1978.

Mende, S. B., J. L. Burch, G. R. Swenson, E. K. Aamodt, S. P. Geller, R. L. Rairden, and P. L. Hassler, Artificial auroras in the upper atmosphere, 2, Imaging results, *Geophys. Res. Lett., 20*, 495, 1993.

Obayashi, T., et al., Space experiments with particle accelerators, *Science, 225*, 195, 1984.

O'Neil, R. R., F. Bien, D. Burt, J. A. Sandock, and A. T. Stair Jr., Summarizing results of the artificial auroral experiment, Precede, *J. Geophys. Res., 83*, 3273, 1978a.

O'Neil, R. R., O. Shepherd, W. P. Reidy, J. W. Carpenter, T. N. Davis, D. Newell, J. C. Ulwick, and A. T. Stair Jr., Exceed 2 test, an artificial auroral experiment: Ground-based optical measurements, *J. Geophys. Res., 83*, 2381, 1978b.

O'Neil, R. R., E. T. P. Lee, and E. R. Huppi, Auroral O(^{1}S) production and loss processes: Ground-based measurements of the artificial auroral experiment Precede, *J. Geophys. Res., 84*, 823, 1979.

Rees, M. H., G. H. Romick, H. R. Anderson, and R. T. Casserly, Calculation of auroral emissions from measured electron precipitation: Comparison with observations, *J. Geophys. Res., 81*, 5091, 1976.

Sandie, W. G., S. B. Mende, G. R. Swenson, and M. E. Polites, Atmospheric emissions photometric imaging experiment for Spacelab 1, *Opt. Eng., 22*, 756, 1983.

Vallance -Jones, A., *Aurora*, 119 pp., D. Reidel, Norwell, Mass., 1974.

Wilhelm, K., W. Bernstein, P. J. Kellogg, and B. A. Whalen, Fast magnetospheric echoes of energetic electron beams. *J. Geophys. Res., 90*, 491, 1985.

Winckler, J. R., The application of artificial electron beams to magnetospheric research, *Rev. Geophys., 18*, 659, 1980.

Winckler, J. R., et al., Echo 7: An electron beam experiment in the magnetosphere, *EoS Trans. AGU. 70*, 657, 1989.

S. A. Fuselier, S. P. Geller, S. B. Mende, and G. R. Swenson, Lockheed Palo Alto Research Laboratory, Department 91-20, Building 252, 3251 Hanover Street, Palo Alto, CA 94304. (e-mail: mende@sag.space.lockheed.com)

J. A. Marshall, Department of Physics, Utah State University, Logan, UT 84322.

(Received November 8, 1994; revised March 27, 1995;
accepted March 29, 1995.)